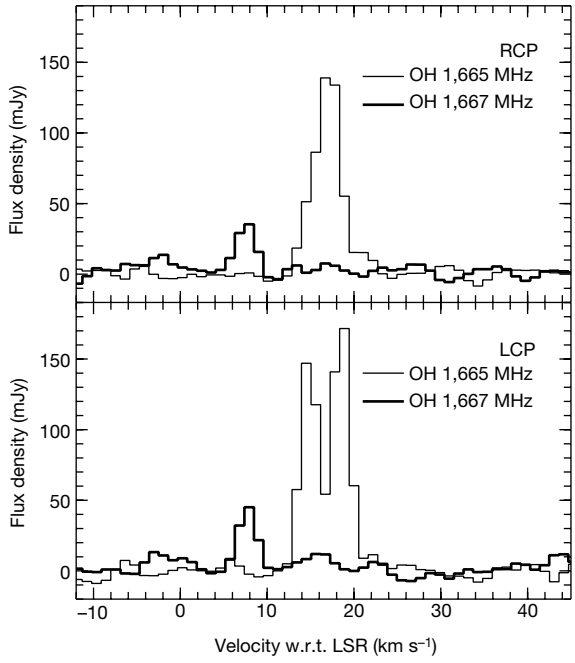

Figure 2 Spectra of the OH 1,665-MHz and 1,667-MHz lines in K3-35. The total velocity range covered by the OH observations was ~140 km s^{-1}. The figure shows the spectra for the left circular polarization (LCP; bottom) and right circular polarization (RCP; top), corresponding to the integrated emission over a region of <1″ in size where all the OH-maser emission detected arises (Fig. 1).

and S requires a shielding mechanism against ionizing radiation. A full understanding of this mechanism will require detailed modelling studies. □

Received 7 June; accepted 27 September 2001.

1. Lewis, B M. The chronological sequence of circumstellar masers: identifying proto-planetary nebulae. *Astrophys. J.* **338,** 234–243 (1989).
2. Elitzur, M. Astronomical masers. *Annu. Rev. Astron. Astrophys.* **30,** 75–112 (1992).
3. Habing, H. J. Circumstellar envelopes and asymptotic giant branch stars. *Astron. Astrophys. Rev.* **7,** 97–207 (1996).
4. Gómez, Y., Moran, J. M. & Rodríguez, L. F. H_2O and SiO maser emission in OH/IR stars. *Rev. Mex. Astron. Astrophys.* **20,** 55–66 (1990).
5. Aaquist, O. B. Detailed radio morphology of the compact nebula K3-35. *Astron. Astrophys.* **267,** 260–264 (1993).
6. Miranda, L. F. *et al.* High-resolution spectroscopy and broad-band imaging of the young planetary nebula K3-35. *Mon. Not. R. Astron. Soc.* **311,** 748–754 (2000).
7. Zhang, C. Y. A statistical distance scale for galactic planetary nebulae. *Astrophys. J. Suppl. Ser.* **98,** 659–678 (1995).
8. Kohoutek, L. Hamburg Schmidt-camera survey of faint planetary nebulae. *Bull. Astron. Inst. Czech.* **16,** 221–226 (1965).
9. Engels, D., Schmid-Burgk, J., Walmsley, C. M. & Winnberg, A. K3-35: planetary nebula or compact HII region? *Astron. Astrophys.* **148,** 344–346 (1985).
10. Aaquist, O. B. & Kwok, S. Bipolar radio morphology in the compact nebula K3-35. *Astron. Astrophys.* **222,** 227–230 (1989).
11. Dayal, A. & Bieging, J. H. Millimeter-wave observations of CO in planetary nebulae. *Astrophys. J.* **472,** 703–710 (1996).
12. Acker, A. Interactive winds in low-mass evolved stars. *Astrophys. Space Sci.* **260,** 185–198 (1998).
13. Evans, I. N. & Dopita, M. A. Theoretical models for HII regions. I. Diagnostic diagrams. *Astrophys. J. Suppl. Ser.* **58,** 125–142 (1985).
14. Raga, A. C., Böhm, K.-H. & Cantó, J. A compilation of optical spectrophotometry of HH objects and its tentative interpretation. *Rev. Mex. Astron. Astrofis.* **32,** 161–174 (1996).
15. Pottasch, S. R. *Planetary Nebulae* (Reidel, Dordrecht, 1984).
16. Acker, A., Marcout, J., Ochsenbein, F., Stenholm, B. & Tylenda, R. *Strasbourg-ESO Catalogue of Galactic Planetary Nebulae* (ESO, Garching, 1992).
17. Zijlstra, A. A. *et al.* OH maser emission from young planetary nebulae. *Astron. Astrophys.* **217,** 157–178 (1989).
18. Spencer, J. H., Johnston, K. J., Moran, J. M., Reid, M. J. & Walker, R. C. The structure of H_2O masers associated with late-type stars. *Astrophys. J.* **230,** 449–455 (1979).
19. Marvel, K. B. The circumstellar environment of evolved stars as revealed by studies of circumstellar water masers. *Publ. Astron. Soc. Pacif.* **109,** 1286–1287 (1997).
20. Bowers, P. F. & Morris, M. The three-dimensional structure of a circumstellar maser. *Astrophys. J.* **276,** 646–652 (1984).
21. Likkel, L. & Morris, M. The circumstellar water fountains of IRAS 16342-3814: a very high velocity bipolar outflow. *Astrophys. J.* **329,** 914–919 (1988).
22. Marvel, K. B. & Boboltz, D. A. Observations of water masers associated with the proto-planetary nebula candidate IRAS 19296+2227. *Astron. J.* **118,** 1791–1797 (1999).
23. Goldreich, P., Keeley, D. A. & Kwan, J. Y. Astrophysical masers II. Polarization properties. *Astrophys. J.* **179,** 111–134 (1973).
24. Cohen, R. J. Compact maser sources. *Rep. Prog. Phys.* **52,** 881–943 (1989).
25. Blackman, E. G., Frank, A., Markiel, J. M., Thomas, J. H. & Van Horn, H. M. Dynamos in asymptotic-giant-branch stars as the origin of magnetic fields shaping planetary nebulae. *Nature* **409,** 485–487 (2001).
26. Hu, J. Y., Slijkhuis, S., Rieu, N.-Q. & de Jong, T. IRAS 17150-3224: a young, optically bipolar, proto-planetary nebula. *Astron. Astrophys.* **273,** 185–193 (1993).
27. Rozyczka, M. & Franco, J. Toroidal magnetic fields and the evolution of wind-driven nebulae. *Astrophys. J.* **469,** L127–L130 (1996).
28. Elitzur, M., Hollenbach, D. J. & McKee, C. F. H_2O masers in star-forming regions. *Astrophys. J.* **346,** 983–990 (1989).
29. Zijlstra, A. *et al.* Bipolar outflows in OH/IR stars. *Mon. Not. R. Astron. Soc.* **322,** 280–308 (2001).
30. Elitzur, M., Hollenbach, D. J. & McKee, C. F. Planar H_2O masers in star-forming regions. *Astrophys. J.* **394,** 221–227 (1992).

Acknowledgements

We thank L. F. Rodríguez and P. Ho for comments. NRAO is a facility of the National Science Foundation operated under cooperative agreement by Associated Universities, Inc. G.A., L.F.M. and J.M.T. are supported partially by MCYT, Spain. Y.G. acknowledges support from DGAPA, UNAM and CONACyT, Mexico. G.A. acknowledges support from MEC, Spain.

Correspondence and requests for materials should be addressed to L.F.M. (e-mail: lfm@iaa.es).

How many-particle interactions develop after ultrafast excitation of an electron–hole plasma

R. Huber*, F. Tauser*, A. Brodschelm*, M. Bichler†, G. Abstreiter† & A. Leitenstorfer*

* *Physik-Department E11, Technische Universität München, James-Franck-Strasse, D-85748 Garching, Germany*
† *Walter-Schottky-Institut, Technische Universität München, Am Coulombwall, D-85748 Garching, Germany*

Electrostatic coupling between particles is important in many microscopic phenomena found in nature. The interaction between two isolated point charges is described by the bare Coulomb potential, but in many-body systems this interaction is modified as a result of the collective response of the screening cloud surrounding each charge carrier[1,2]. One such system involves ultrafast interactions between quasi-free electrons in semiconductors[3,4]—which are central to high-speed and future quantum electronic devices. The femtosecond kinetics of non-equilibrium Coulomb systems has been calculated using static[5,6] and dynamical[7,8] screening models that assume the instantaneous formation of interparticle correlations. However, some quantum kinetic theories[9–14] suggest that a regime of unscreened bare Coulomb collisions might exist on ultrashort timescales. Here we monitor directly the temporal evolution of the charge–charge interactions after ultrafast excitation of an electron–hole plasma in GaAs. We show that the onset of collective behaviour such as Coulomb screening and plasmon scattering exhibits a distinct time delay of the order of the inverse plasma frequency, that is, several 10^{-14} seconds.

The plasma state is often called the fourth state of matter, in addition to solids, liquids and gases. In a plasma, charged particles such as electrons and ions or nuclei are no longer bound together as atoms, molecules or solid-state crystals. The charge carriers are free to move and respond independently to electromagnetic fields. In

momentum space, the interaction between two isolated elementary charges e is given by the bare Coulomb potential V_q (ref. 1):

$$V_q = \frac{4\pi e^2}{q^2} \quad (1)$$

We note that V_q depends solely on the momentum exchange q of the two particles during a collision. In a many-body system, the bare Coulomb potential becomes modified as a result of collective effects: each negative charge attracts a cloud of positive charges and vice versa. The combination of a charge carrier and the surrounding screening cloud is commonly referred to as a 'dressed' quasi-particle. The effective screened interaction potential $W_q(\omega, t_D)$ may be expressed as[1,2]:

$$W_q(\omega, t_D) = \frac{V_q}{\epsilon_q(\omega, t_D)} \quad (2)$$

where V_q is renormalized via the longitudinal dielectric function $\epsilon_q(\omega, t_D)$. $W_q(\omega, t_D)$ depends on the energy $\hbar\omega$ exchanged in a collision. Correspondingly, the dressed interaction is no longer instantaneous. It becomes time-dependent owing to the retarded response of the polarization cloud. The retardation is a result of a resonance of the entire many-body system at the plasma frequency ω_{pl}, which is directly proportional to the square root of the particle pair density N divided by the reduced effective mass m^*. For a nonequilibrium situation, the interaction will also depend upon the time delay t_D with respect to a short perturbation.

Here we address the following question: how quickly are dressed quasi-particles formed, in the case of an initially uncorrelated many-body system of bare particles? Such ultrafast transient phenomena have been suggested to be important in a variety of nonequilibrium systems. Examples range from unscreened positive charges in metals which may influence surface chemistry[15] to the retarded formation of correlations in strongly perturbed nuclear matter[16]. We directly observe the build-up of Coulomb correlations and the formation of dressed quasi-particles in a photoexcited electron–hole plasma in the semiconductor GaAs. This model situation has been studied in theory via quantum kinetic calculations for the nonequilibrium many-body system[9–14]. Experimental access to nonequilibrium dynamics in semiconductors is provided by ultrafast laser spectroscopy[3,4]. Recent experiments exploring the regime of Coulomb quantum kinetics[17–21] have probed the particle distributions and interband polarizations. The time evolution of these quantities contains the scattering in an integral manner. It is less sensitive to the exact form of the interaction potential. In order to study the build-up of screening itself, the low-energy excitations of the plasma and the resulting resonances in $\epsilon_q(\omega, t_D)$ must be measured directly with femtosecond temporal resolution ($1\,\text{fs} = 10^{-15}\,\text{s}$). For the stationary case of doped semiconductors, these plasmons may be observed with classical infrared[22] and light scattering (ref. 23 and see ref. 24 for an overview) techniques. The transient infrared properties of a photoinduced electron–hole plasma have been studied for frequencies below 3 THz ($1\,\text{THz} = 10^{12}\,\text{Hz}$)[25,26] and above 75 THz (ref. 27), with a limited time resolution of 150 fs.

We investigated the evolution of the complex dielectric function renormalizing the bare Coulomb potential (see equation (2)) in the extremely early stage after creation of a nonequilibrium plasma. The principle of our experiment is sketched in Fig. 1. First, free electron–hole pairs are created in a GaAs film via interband transitions

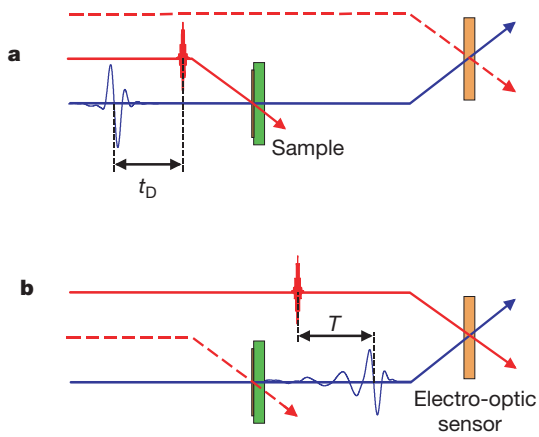

Figure 1 The experimental principle. **a**, First, a thin GaAs sample is excited with a 10-fs laser pulse (red line) at 800 nm, resonant to the interband transition. The sample consists of a 200-nm epitaxial layer of high-purity GaAs ⟨100⟩ on diamond (green block). A single-cycle terahertz electric-field transient (blue line, duration of 27 fs) probes the polarization response of the excited electron–hole plasma after a delay time t_D. The terahertz probe transient is generated via phase-matched optical rectification of a 10-fs visible pulse in a GaSe nonlinear crystal as thin as 30 μm (ref. 28). **b**, Second, the transmitted THz field is measured as a function of time T via ultrabroadband electro-optic sampling in a ⟨110⟩ oriented ZnTe crystal (orange block) of a thickness of 10 μm (refs 29 and 30).

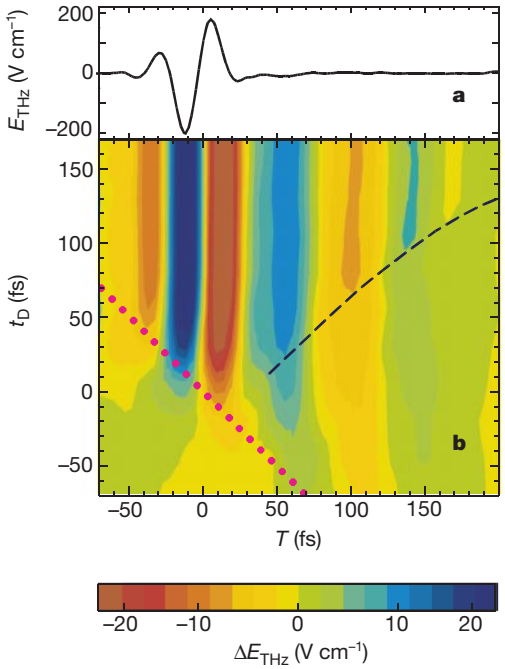

Figure 2 Two-time dependent polarization response of the electron–hole plasma. **a**, Electric-field amplitude E_{THz} of the single-cycle probe versus time T. The transient has been corrected for the frequency response of the electro-optic detector[30]. The Fourier amplitude spectrum contains components between 1 THz and 100 THz, spanning the entire mid- and far-infrared wavelength region from $\lambda = 300$ μm to 3 μm. The phase spectrum is flat between 10 THz and 55 THz. For this frequency interval, the single-cycle pulse represents the ultimate probe with a time resolution limited only by the uncertainty principle. **b**, Electric-field change ΔE_{THz} induced by 10-fs photoexcitation of $2 \times 10^{18}\,\text{cm}^{-3}$ electron–hole pairs in GaAs versus delay times t_D and T. The diagonal pink dotted line denotes the position of the maximum of the 10-fs pump pulse. For pump-probe delays between $t_D = -20$ fs and +20 fs, the excitation pulse overlaps with the electric field of the terahertz probe and a negative (red) and positive (blue) half cycle in ΔE_{THz} appear along the excitation diagonal. These strong features in the vertical region around $T = 0$ fs correspond to an instantaneous perturbation of the single-cycle probe. A retarded oscillatory response of the plasma starts to develop at $t_D = 30$ fs, visualized by the dashed black line to guide the eye: An additional half cycle in ΔE_{THz} builds up, represented by a vertical blue column at $T = 60$ fs. In this region no probe field is present without excitation (see Fig. 2a). For even longer pump-probe delays $t_D > 70$ fs, a second half wave (orange) appears in the retarded response at $T = 100$ fs. Finally, another maximum shows up at $T = 140$ fs, above the $t_D = 100$ fs horizontal and a last minimum appears at $T = 170$ fs for $t_D \geq 120$ fs.

induced with a resonant light pulse (shown red in Fig. 1) of a duration of 10 fs and a central photon energy of 1.55 eV. The photoinduced particle pair density is $N = 2 \times 10^{18}$ cm^{-3}, resulting in a plasma frequency of $\omega_{pl}/2\pi \approx 15$ THz. The properties of this nonequilibrium system are subsequently probed by a different pulse, a single-cycle electric field transient with a duration of 27 fs (full-width at half-maximum, FWHM, of the intensity) and a centre frequency of 28 THz (sketched blue in Fig. 1)[28]. This pulse serves as an extremely short probe pulse for the field response of the semiconductor at a time delay t_D after excitation of the plasma and in the limit of small wave vectors q. Any resonance in the system will manifest itself as a retarded 'tail' owing to induced polarization and a phase distortion of the probe transient after transmission through the sample. As we shall see, the changes induced in the probe electric field contain direct information on the many-body effects renormalizing the bare Coulomb interaction. These changes are directly measured in the time domain in a second stage of the experiment (see Fig. 1b). A third laser pulse with a duration of 10 fs analyses the terahertz wave form of the transmitted probe field as a function of a second delay time T via free-space electro-optic sampling[29,30].

The observed electric field amplitude E_{THz} of the terahertz probe transmitted through the unexcited GaAs sample versus delay time T is shown in Fig. 2a. The terahertz electric field change ΔE_{THz} due to carrier excitation with the 10-fs pump is displayed in a colour map versus pump-probe delay t_D (vertical) and terahertz sampling delay T (horizontal) in Fig. 2b. The polarization response of the carrier plasma follows instantaneously upon the single-cycle probe pulse at early delay times t_D between −20 fs and 20 fs. With increasing values of t_D the plasma develops a delayed oscillatory response after the terahertz probe burst: starting with a first retarded half wave for $t_D = 30$ fs, up to two delayed full oscillation cycles are observed for $t_D \geq 120$ fs. At pump-probe delays beyond $t_D = 150$ fs, the electric field change ΔE_{THz} versus T becomes stationary on a picosecond timescale determined by the carrier recombination time in the sample.

In order to analyse further the amplitude- and phase-resolved data of Fig. 2 and to extract the complex $\epsilon_{q=0}(\omega, t_D)$, we performed an incomplete Fourier transform[11,25] into the frequency domain only along the terahertz response axis T. The imaginary and real parts of the deduced inverse dielectric function are shown versus frequency for different pump-probe delays t_D in Fig. 3a and b, respectively. These data demonstrate the build-up of the dressed interaction in the many-body system with respect to the initial bare Coulomb potential V_q. On top of Fig. 3, the frequency scale has been multiplied by Planck's constant in order to convert into the energy $\hbar\omega$ exchanged in a collision between particles. We start our discussion with the negative imaginary part of $1/\epsilon_{q=0}$, which is a measure for the energy loss of a charged particle propagating in the many-body system. We note that the bare Coulomb interaction of equation (1) lacks an imaginary part. As a consequence, $-\mathrm{Im}(1/\epsilon_{q=0})$ vanishes exactly for the unexcited system (green line in Fig. 3a), except for a small peak at $\omega_{LO}/2\pi = 8.8$ THz, the frequency of the longitudinal optical phonon. This feature comes from the fact that even a single electron in GaAs may exchange the energy quantum $\hbar\omega_{LO} = 36$ meV with the crystal lattice by polar-optical scattering[31]. When the electron–hole plasma is injected at $t_D = 0$ fs, the resonance shifts to higher energies and becomes strongly broadened. The maximum spectral width is obtained at a pump-probe delay of $t_D = 25$ fs. At this point, a wide range of energies may be exchanged between the charge carriers, indicating an uncorrelated state in an extreme nonequilibrium situation. Within 100 fs, the broad feature narrows significantly and a sharp resonance in $-\mathrm{Im}(1/\epsilon_{q=0})$ appears at a plasma frequency of $\omega_{pl}/2\pi = 14.4$ THz (Fig. 3a). We observe the transition to a collective response of the many-body system: The carrier dynamics becomes dominated by scattering with plasmons, the energy quanta of the plasma oscillation, of an energy of $\hbar\omega_{pl} = 60$ meV.

The build-up of a dressed Coulomb interaction is well described by the real part of the inverse dielectric function in Fig. 3b. This quantity renormalizes the charge that an electron is affected by while interacting with another quasi-particle in the plasma, exchanging an energy $\hbar\omega$; see equations (1) and (2). For late pump-probe delays of $t_D > 150$ fs, a negative minimum is found for frequencies below the plasma frequency. Obviously, the effective interaction in equation (2) changes sign for an energy exchange slightly below $\hbar\omega_{pl}$. This phenomenon is due to the oppositely charged screening cloud surrounding the bare particle which is excited resonantly and dominates the collision. In contrast, $\mathrm{Re}(1/\epsilon_{q=0})$ has a positive maximum at energies slightly above $\hbar\omega_{pl}$: if the plasma is driven above resonance, the polarization oscillates out of phase with the electromagnetic perturbation. As a result, the Coulomb forces due to the bare charge and the screening cloud add up with the same sign. These features are consistent with a fully

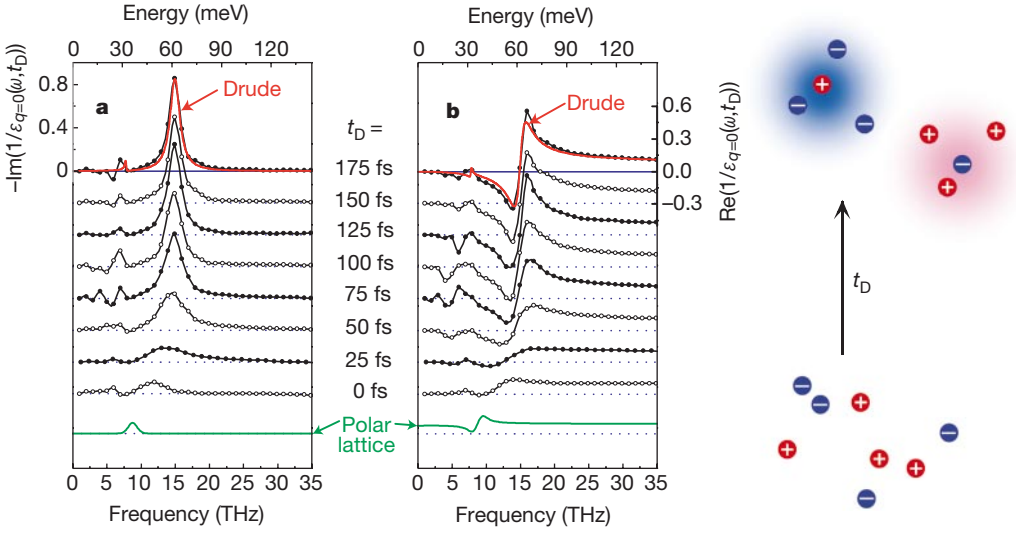

Figure 3 Build-up of Coulomb screening and plasmon scattering. **a**, **b**, Imaginary (**a**) and real (**b**) part of the long-wavelength limit of the inverse dielectric function of GaAs versus frequency for different pump-probe delays t_D, as deduced from the time-domain data in Fig. 2. The green lines result from a dielectric oscillator model for unexcited GaAs. A Drude fit of the data at $t_D = 175$ fs ($\tau = 84$ fs and $\omega_{pl} = 14.4$ THz) is drawn red. The sketch on the right visualizes the transition from a chaotic system of bare charges to an ensemble of correlated screened quasi-particles. Dotted lines are offset zero lines (blue).

developed dressed interaction. We note that the extrema around ω_{pl} in $\mathrm{Re}(1/\epsilon_{q=0})$ originating from anti- and over-screening do not emerge instantaneously with carrier generation but show a delayed rise within the first 120 fs. At $t_D = 25$ fs, the spectrum is completely flat above $\hbar\omega_{pl}$, indicating bare Coulomb collisions without any screening.

The classical model for the long-wavelength and high-frequency limit of the dielectric function of an electron gas is given by Drude theory[1,32], assuming an exponential plasmon damping with a time constant τ. We performed least-square fits to our data allowing ω_{pl} and τ as free parameters and keeping the lattice part fixed. Good agreement with a Drude shape is found only for late delay times with $\omega_{pl} = 14.4$ THz at $t_D = 175$ fs (see red curves in Fig. 3). τ is a measure for the memory depth of the system and for the duration of a collision. It increases from $\tau \approx 20$ fs at $t_D = 25$ fs to $\tau = 85$ fs for $t_D \geq 120$ fs. Our experimental findings support quantum kinetic theories for the nonequilibrium dynamics of the Coulomb interaction[10–14]. These models predict a delayed build-up of screening and a strongly broadened plasmon pole after ultrafast excitation. The approximate timescale for these phenomena is linked to the duration of a plasma oscillation period which is $2\pi/\omega_{pl} = 70$ fs in our experiment.

Thus, we have demonstrated a direct test for a basic concept in nonequilibrium many-body physics: the formation of dressed quasi-particles. We show that Coulomb screening and plasmon scattering are not present instantaneously after 10-fs photoexcitation of a dense electron–hole plasma in GaAs, but emerge on a timescale comparable to the inverse plasma frequency. This class of phenomena marks the earliest stage in the dynamics of strongly perturbed particle ensembles far from equilibrium. The results are obtained by applying a new technique, where the polarization response of the system to a single-cycle electric field transient covering the entire mid infrared is directly resolved. The dynamics of elementary excitations in this important spectral region can now be accessed with uncertainty-limited femtosecond resolution of both amplitude and phase. New perspectives arise for investigations in systems such as magnons in high-T_c superconductors, lattice dynamics in organic semiconductors, and vibrational relaxation in large molecules and biological complexes. □

Received 14 June; accepted 18 September 2001.

1. Mahan, G. D. *Many-Particle Physics* 2nd edn (Plenum, New York, 1993).
2. Lindhard, J. On the properties of a gas of charged particles. *Dan. Mat.-fys. Medd.* **28,** 2–57 (1954).
3. Shah, J. *Ultrafast Spectroscopy of Semiconductors and Semiconductor Nanostructures* 2nd edn (Springer, Berlin, 1999).
4. Chemla, D. S. & Shah, J. Many-body and correlation effects in semiconductors. *Nature* **411,** 549–557 (2001).
5. Osman, M. A. & Ferry, D. K. Monte Carlo investigation of the electron–hole-interaction effects on the ultrafast relaxation of hot photoexcited carriers in GaAs. *Phys. Rev. B* **36,** 6018–6032 (1987).
6. Goodnick, S. M. & Lugli, P. Effect of electron–electron scattering on nonequilibrium transport in quantum-well systems. *Phys. Rev. B* **37,** 2578–2588 (1988).
7. Young, J. F., Henry, N. L. & Kelly, P. J. Full dynamical screening calculation of hot electron scattering rates in multicomponent semiconductor plasma. *Solid State Electron.* **32,** 1567–1571 (1989).
8. Collet, J. H. Dynamical screening in the cooling theory of high-density electron–hole plasmas. *Phys. Rev. B* **39,** 7659–7665 (1989).
9. Haug, H. & Jauho, A.-P. *Quantum Kinetics in Transport and Optics of Semiconductors* (Springer, Berlin, 1996).
10. Hartmann, M., Stolz, H. & Zimmermann, R. Kinetics of screening in optically excited semiconductors. *Phys. Status Solidi B* **159,** 35–42 (1990).
11. El Sayed, K., Schuster, S., Haug, H., Herzel, F. & Henneberger, K. Subpicosecond plasmon response: Buildup of screening. *Phys. Rev. B* **49,** 7337–7344 (1994).
12. Bányai, L., Vu, Q. T., Mieck, B. & Haug, H. Ultrafast quantum kinetics of time-dependent RPA-screened coulomb scattering. *Phys. Rev. Lett.* **81,** 882–885 (1998).
13. Kwong, N.-H. & Bonitz, M. Real-time Kadanoff-Baym approach to plasma oscillations in a correlated electron gas. *Phys. Rev. Lett.* **84,** 1768–1771 (2000).
14. Vu, Q. T. & Haug, H. Time-dependent screening of the carrier–phonon and carrier–carrier interactions in non-equilibrium systems. *Phys. Rev. B* **62,** 7179–7185 (2000).
15. Schöne, W.-D. & Ekardt, W. Time-dependent screening of a positive charge distribution in metals: Excitons on an ultrashort time scale. *Phys. Rev. B* **62,** 13464–13471 (2000).
16. Köhler, H. S. Memory and correlation effects in nuclear collisions. *Phys. Rev. C* **51,** 3232–3239 (1995).
17. Camescasse, F. X. *et al.* Ultrafast electron redistribution through Coulomb scattering in undoped GaAs: Experiment and theory. *Phys. Rev. Lett.* **77,** 5429–5432 (1996).
18. Hügel, W. A. *et al.* Photon echoes from semiconductor band-to-band continuum transitions in the regime of Coulomb quantum kinetics. *Phys. Rev. Lett.* **83,** 3313–3316 (1999).
19. Bolton, S. R., Neukirch, U., Sham, L. J., Chemla, D. S. & Axt, V. M. Demonstration of sixth-order Coulomb correlations in a semiconductor single quantum well. *Phys. Rev. Lett.* **85,** 2002–2005 (2000).
20. Vu, Q. T., Haug, H., Hügel, W. A., Chatterjee, S. & Wegener, M. Signature of electron-plasmon quantum kinetics in GaAs. *Phys. Rev. Lett.* **85,** 3508–3511 (2000).
21. Bonitz, M., Lampin, J. F., Camescasse, F. X. & Alexandrou, A. Nonequilibrium plasmons in optically excited semiconductors. *Phys. Rev. B* **62,** 15724–15734 (2000).
22. Spitzer, W. G. & Fan, H. Y. Determination of optical constants and carrier effective masses of semiconductors. *Phys. Rev.* **106,** 882–890 (1957).
23. Mooradian, A. & Wright, G. B. Observation of the interaction of plasmons with longitudinal optical phonons in GaAs. *Phys. Rev. Lett.* **16,** 999–1001 (1966).
24. Abstreiter, G., Cardona, M. & Pinczuk, A. Light scattering by free carrier excitations in semiconductors. *Springer Topics Appl. Phys.* **54,** 5–150 (1984).
25. Schall, M. & Jepsen, P. U. Photoexcited GaAs surfaces studied by transient terahertz time-domain spectroscopy. *Opt. Lett.* **25,** 13–15 (2000).
26. Beard, M. C., Turner, G. M. & Schmuttenmaer, C. A. Transient photoconductivity in GaAs as measured by time-resolved terahertz spectroscopy. *Phys. Rev. B* **62,** 15764–15777 (2000).
27. Ganikhanov, F., Burr, K. C., Hilton, D. J. & Tang, C. L. Femtosecond optical-pulse-induced absorption and refractive-index changes in GaAs in the midinfrared. *Phys. Rev. B* **60,** 8890–8896 (1999).
28. Huber, R., Brodschelm, A., Tauser, F. & Leitenstorfer, A. Generation and field-resolved detection of femtosecond electromagnetic pulses tunable up to 41 THz. *Appl. Phys. Lett.* **76,** 3191–3193 (2000).
29. Wu, Q. & Zhang, X.-C. Free-space electro-optic sampling of mid-infrared pulses. *Appl. Phys. Lett.* **71,** 1285–1286 (1997).
30. Leitenstorfer, A., Hunsche, S., Shah, J., Nuss, M. C. & Knox, W. H. Detectors and sources for ultrabroadband electro-optic sampling: Experiment and theory. *Appl. Phys. Lett.* **74,** 1516–1518 (1999).
31. Fürst, C., Leitenstorfer, A., Laubereau, A. & Zimmermann, R. Quantum kinetic electron-phonon interaction in GaAs: Energy non-conserving scattering events and memory effects. *Phys. Rev. Lett.* **78,** 3733–3736 (1997).
32. Yu, P. Y. & Cardona, M. *Fundamentals of Semiconductors* (Springer, Berlin, 1996).

Acknowledgements

We thank H. Haug, W. Kaiser, L. V. Keldysh and A. Laubereau for discussions and continuous support.

Correspondence and requests for materials should be addressed to A.L. (e-mail: aleitens@ph.tum.de).

On-chip natural assembly of silicon photonic bandgap crystals

Yurii A. Vlasov*†, Xiang-Zheng Bo‡, James C. Sturm‡ & David J. Norris*

**NEC Research Institute, 4 Independence Way, Princeton, New Jersey 08540, USA*
† A. F. Ioffe Physical-Technical Institute, St. Petersburg, Russia
‡ Department of Electrical Engineering and Center for Photonics and Optoelectronic Materials, Princeton University, Princeton, New Jersey 08544, USA

Photonic bandgap crystals can reflect light for any direction of propagation in specific wavelength ranges[1–3]. This property, which can be used to confine, manipulate and guide photons, should allow the creation of all-optical integrated circuits. To achieve this goal, conventional semiconductor nanofabrication techniques have been adapted to make photonic crystals[4–9]. A potentially simpler and cheaper approach for creating three-dimensional periodic structures is the natural assembly of colloidal microspheres[10–15]. However, this approach yields irregular, polycrystalline photonic crystals that are difficult to incorporate into a device. More importantly, it leads to many structural defects that can destroy the photonic bandgap[16,17]. Here we show that by assembling a thin layer of colloidal spheres on a silicon substrate, we can obtain planar, single-crystalline silicon photonic crystals that have defect densities sufficiently low that the bandgap survives. As expected from theory, we observe unity reflectance in two crystalline directions of our photonic crystals around a wavelength of 1.3 micrometres. We also show that additional fabrication steps, intentional doping and patterning, can be performed, so demonstrating the potential for specific device applications.

The strategy behind the colloidal assembly approach is to exploit the tendency of monodisperse submicrometre spheres to sponta-